MICROCOPY RESOLUTION TEST CHART

NATIONAL BUREAU OF STANDARDS 1963 A

JFM

④

Observation of Nonlinear Wave Decay Processes
in the Solar Wind
by the AMPTE IRM Plasma Wave Experiment

AD-A191 409

H. C. KOONS and J. L. ROEDER
Space Sciences Laboratory
The Aerospace Corporation
El Segundo, CA 90245

O. H. BAUER, G. HAERENDEL and R. TREUMANN
Max-Planck-Institute for Physics and Astrophysics
Institute for Extraterrestrial Physics
8046 Garching by Munich
Federal Republic of Germany

R. R. ANDERSON and D. A. GURNETT
Department of Physics and Astronomy
University of Iowa
Iowa City, IA 52242

R. H. HOLZWORTH
University of Washington
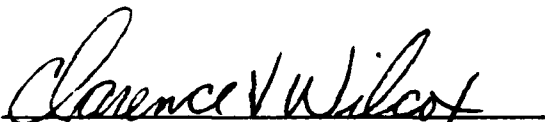Space Sciences Division
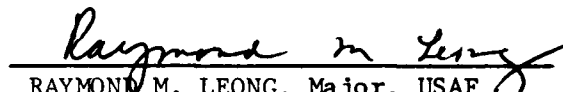Seattle, WA 98195

5 February 1988

DTIC

APR

H

88 4 4 126

This report was submitted by The Aerospace Corporation, El Segundo, CA 90245, under Contract No. F04701-85-C-0086 with the Space Division, P.O. Box 92960, Worldway Postal Center, Los Angeles, CA 90009-2960. It was reviewed and approved for The Aerospace Corporation by H. R. Rugge, Director, Space Sciences Laboratory. Lt Clarence V. Wilcox, CLTPC was the project officer for the Mission-Oriented Investigation and Experimentation (MOIE) Program.

This report has been reviewed by the Public Affairs Office (PAS) and is releasable to the National Technical Information Service (NTIS). At NTIS, it will be available to the general public, including foreign nationals.

This technical report has been reviewed and is approved for publication. Publication of this report does not constitute Air Force approval of the report's findings or conclusions. It is published only for the exchange and stimulation of ideas.

CLARENCE V. WILCOX, Lt, USAF
MOIE Project Officer
SD/CLTPC

RAYMOND M. LEONG, Major, USAF
Deputy Director, AFSTC West Coast Office
AFSTC/WCO OL-AB

REPORT DOCUMENTATION PAGE

1a REPORT SECURITY CLASSIFICATION	1b RESTRICTIVE MARKINGS
Unclassified	

2a SECURITY CLASSIFICATION AUTHORITY	3 DISTRIBUTION/AVAILABILITY OF REPORT
	Approved for public release;
2b DECLASSIFICATION/DOWNGRADING SCHEDULE	distribution unlimited.

4 PERFORMING ORGANIZATION REPORT NUMBER(S)	5 MONITORING ORGANIZATION REPORT NUMBER(S)
TR-0086(6940-06)-14	SD-TR-88-18

6a NAME OF PERFORMING ORGANIZATION	6b OFFICE SYMBOL (If applicable)	7a NAME OF MONITORING ORGANIZATION
The Aerospace Corporation Laboratory Operations		Space Division Los Angeles Air Force Base

6c ADDRESS (City, State, and ZIP Code)	7b ADDRESS (City, State, and ZIP Code)
El Segundo, CA 90245	Los Angeles, CA 90009-2960

8a NAME OF FUNDING/SPONSORING ORGANIZATION	8b OFFICE SYMBOL (If applicable)	9 PROCUREMENT INSTRUMENT IDENTIFICATION NUMBER
		F04701-85-C-0086

8c ADDRESS (City, State, and ZIP Code)	10 SOURCE OF FUNDING NUMBERS			
	PROGRAM ELEMENT NO.	PROJECT NO.	TASK NO	WORK UNIT ACCESSION NO.

11 TITLE (Include Security Classification)

Observations of Nonlinear Wave Decay Processes in the Solar Wind by the AMPTE IRM Plasma Wave Experiment

12 PERSONAL AUTHOR(S) Koons, H.C., Roeder, J.L.; Bauer, O.H., Haerendel, G., Treumann, R. (Max-Planck-Institute for Physics and Astrophysics); Anderson, R.R., Gurnett, D.A. (University

13a TYPE OF REPORT	13b TIME COVERED FROM _____ TO _____	14 DATE OF REPORT (Year, Month, Day) 1988 February 5	15 PAGE COUNT 33

16 SUPPLEMENTARY NOTATION

17 COSATI CODES			18 SUBJECT TERMS (Continue on reverse if necessary and identify by block number)
FIELD	GROUP	SUB-GROUP	Plasma frequency, Langmuir waves
			Ion acoustic wave

19 ABSTRACT (Continue on reverse if necessary and identify by block number)

Nonlinear wave decay processes have been detected in the solar wind by the plasma wave experiment aboard the AMPTE-IRM spacecraft. The main process is the generation of ultra-low-frequency ion-acoustic waves from the decay of Langmuir waves near the electron plasma frequency. Frequently this is accompanied by an enhancement of emissions near twice the plasma frequency. This enhancement is most likely due to the generation of electromagnetic waves from the coalescence of two Langmuir waves. These processes occur within the electron foreshock in front of the earth's bow shock.

20 DISTRIBUTION/AVAILABILITY OF ABSTRACT	21 ABSTRACT SECURITY CLASSIFICATION
☑ UNCLASSIFIED/UNLIMITED ☐ SAME AS RPT ☐ DTIC USERS	Unclassified
22a NAME OF RESPONSIBLE INDIVIDUAL	22b TELEPHONE (Include Area Code) 22c OFFICE SYMBOL

DD FORM 1473, 84 MAR 83 APR edition may be used until exhausted   SECURITY CLASSIFICATION OF THIS PAGE
All other editions are obsolete

Item 12. Continued.

of Iowa);   and Holzworth, R.H. (University of Washington).

PREFACE

1

CONTENTS

FIGURES

I. INTRODUCTION

A variety of astrophysical phenomena are believed to arise from nonlinear plasma wave decay processes. These include narrow band radiation near the second harmonic of the plasma frequency (f_p) from a location near the earth's bow shock[1] and, similarly, the generation of transverse waves at $2f_p$ in the solar wind as type III solar radio bursts.[2] The mechanism for the generation of the transverse waves near $2f_p$ is generally believed to be the coalescence of two Langmuir waves.[2,3,4] Theory requires an intermediate ion acoustic wave to accomplish the process.

The intermediate ion acoustic wave can participate in either a down-conversion or an up-conversion process. We adopt the nomenclature used by Cairns and Melrose[4] where L and L' represent Langmuir waves, S represents the ion acoustic wave, and T represents the transverse (electromagnetic) wave at $2f_p$. The first possibility involves the decay or down conversion of a Langmuir wave, L, into an ion acoustic wave and a backward- traveling Langmuir wave, L', followed by the coalescence of the two Langmuir waves into a transverse wave. Symbolically this is represented by the equation:

$$L = L' + S$$
$$L + L' = T$$

Observations would show the generation of ion acoustic waves in conjunction with an enhancement in the intensity and an increase in the bandwidth of Langmuir waves and the appearance of transverse waves.

The second possibility is the coalescence or up conversion of an ion acoustic wave and a Langmuir wave, L, to form a backward traveling Langmuir wave, L'. The two Langmuir waves would then coalesce to form the transverse wave.

$$L + S = L'$$
$$L + L' = T$$

Observations would show an absorption of ion acoustic waves in conjunction with a broadening of the spectrum of the Langmuir waves and the appearance of transverse waves.

Previous spacecraft have observed ion acoustic waves in the vicinity of the bow shock in the region from which the $2f_p$ radiation was detected.[5] Although this supports the role of acoustic waves in the generation process, it does not distinguish between the two possible generation mechanisms.

Data from the stepped frequency receiver (SFR) aboard the AMPTE IRM spacecraft supports the decay process as the mechanism for the generation of transverse waves at twice the electron plasma frequency near the earth's bow shock in the solar wind.

II. INSTRUMENT

The stepped frequency receiver (SFR) is part of the plasma wave instrument on the AMPTE IRM spacecraft. For a description of the entire plasma wave instrument see Häusler et al.[6] The SFR simultaneously operates over three linear frequency bands that cover the frequency range from 200 Hz to 100 kHz. The low- frequency band covers 200 Hz to 2.5 kHz. The mid-frequency band covers 1 kHz to 10 kHz and the high-frequency band covers 10 kHz to 100 kHz. The instrument can be operated in a variety of modes and sensitivities as described by Häusler et al.[6] The skirts on the filters are very steep. For a 0 dB input signal into the center of a 3 kHz wide channel in the high-frequency band, the adjacent channels will detect a signal at -45 dB.

The plasma wave instrument also contains a wide-band analog receiver. It consists of an automatic-gain-control receiver covering the frequency range from 650 Hz to 10 kHz as a baseband channel, and a frequency-modulated subcarrier at 13.5 kHz which contains a dc compressor output for the frequency range from 5 Hz to 1 kHz. The signal directly modulates the S-band telemetry carrier frequency.

A difficulty with the observation of plasma wave nonlinearities is the inherent nonlinearity of the receivers used to make the measurements. The SFR on the AMPTE IRM has a dynamic range of 60 dB. The upper limit of the range, which can be set at 1 V, 100 mV or 10 mV, was set to 10 mV for the measurements reported in this report. For amplitudes near the upper input level for each range, virtually no nonlinearities are observed in the receiver. However, if this level is exceeded, then harmonic, intermodulation, and interband distortion are observed.

At levels below 3 mV on the 10 mV scale there is essentially no distortion of any type. Although the harmonic distortion is low at 10 mV, it rises rapidly for signals only a few dB above 10 mV. Interband distortion in the instrument shows up in the same channel number in a different frequency band. For example, a strong signal at 51,000 Hz (channel 15) in the high-frequency band can produce a signal at 5,100 Hz (channel 15) in the mid-

7

frequency range. There is no measurable interband distortion below 30 mV on the 10 mV scale. The distortion then rises rapidly but saturates at an output level of 700 mV (full scale is 5.1 V) for input levels above 60 mV.

These types of distortion mimic the natural behavior of the plasma. The instrumental behavior has been carefully compared with the observed data to differentiate the natural processes from the instrumental effects.

III. DATA

Figure 1 is a spectrogram from the SFR showing an example of the decay or down-conversion process observed on November 15, 1984. The top panel, covering the frequency range from 9 kHz to 99 kHz, contains the Langmuir waves (the lower horizontal band in the upper panel) and the transverse waves (the upper horizontal band in the upper panel). The plasma frequency during this time period increased from approximately 25 to 40 kHz at an altitude of 15 earth radii near 1020 local time in the solar wind.

When the plasma line is weak (e.g. from 0640 to 0646 UT), there are only weak emissions below 10 kHz. Each time the plasma line intensifies during the one hour interval shown in the spectrogram, much stronger emissions appear at the low end of the frequency spectrum up to about 3 kHz. The upper cutoff can best be seen in the center panel of the spectrogram in Figure 1. These low-frequency emissions frequently appear at times when the Langmuir waves are well below the levels at which distortion occurs in the instrument. That is the case for the data shown in Figure 1. When the saturation level of the instrument is exceeded, vertical bands appear across the top panel of the spectrogram. An example occurs near 0712 UT in Figure 1. The vertical band from 9 to 99 kHz appears at the times when the strongest Langmuir waves were detected. The remainder of the time the wave amplitudes are below the instrument distortion level.

Figure 2 shows another example at 0811 UT on September 20, 1984. At that time the receiver was operating in a different mode. The middle and bottom panels cover the same frequency range from 0.2 to 2.5 kHz. The middle panel shows the data from the electric antenna and the bottom panel shows the data from the magnetic antenna. The spectrum in the bottom panel shows very weak electromagnetic interference generated by spacecraft timing signals. These signals are near the internal noise level of the receiver, except for the one line at 1 kHz. When the Langmuir line intensifies, there is no evidence for signals in the magnetic channel corresponding with the waves in the low-frequency electric channel.

9

We interpret the waves below 3 kHz to be electrostatic ion acoustic waves generated by the decay process:

$$L = L' + S$$

Figure 3 shows a spectrogram of these emissions from the wide-band receiver for a one minute period from 0810 to 0811 UT on September 20, 1984. The ion acoustic waves associated with the Langmuir waves are the more intense emissions at the bottom of the spectrogram. The emissions at this higher resolution have the appearance of impulses at the low frequency end of the spectrum. The width of each impulse on the spectrogram is approximately 0.1 s. That is the same as the decay time of the Sanders Spectrum Analyzer on the frequency range used in the laboratory to produce the spectrogram. We conclude that the emissions are highly impulsive and probably have not been temporaly resolved.

The spectrogram in Figure 3 also shows a weak, spin-modulated, broadband emission between 500 Hz and 1.5 kHz. The ion-acoustic waves from the decay process are not strongly correlated with the spin-modulation on this broadband noise. This noise may be ion acoustic noise produced by some other process.

The low-frequency waves have been observed to correlate with the intensification of the Langmuir waves on 21 days between September 20 and November 29, 1984. Data from all of the days in that time period have not been reduced and the data base is not yet complete enough to be used to compile statistics on the occurrence of this phenomenon. However, there is sufficient data to indicate that this type of parametric decay is not a rare occurrence.

During several of the observations, there is also an appearance or strengthening of the emission at the second harmonic of the electron plasma frequency in conjunction with the increase in amplitude of the Langmuir waves. Figure 1 shows an example of this, especially from 0659 to 0714 UT. The Langmuir waves increase in amplitude from 10^{-8} to 3×10^{-5} v/m/Hz$^{1/2}$ while the harmonic increases from 10^{-8} to 10^{-7} v/m/Hz$^{1/2}$. For the time periods that are currently available for analysis, the SFR always operated in a mode which

10

collected data above 9 kHz from only the electric antenna. Thus, it is not possible with this data to conclusively determine if the emission at the second harmonic of the plasma frequency is electromagnetic.

Harmonic emissions are difficult to distinguish from an instrumental effect because the Langmuir waves frequently reach levels that are larger than the levels at which harmonic distortion occurs. That is not the case for most of the time period from 0659 to 0714 UT in Figure 1.

Figure 4 shows the signal levels in four different frequency channels during a 100 s time period on October 31, 1984 when there was an enhancement at the harmonic of the plasma frequency in conjunction with enhanced Langmuir waves and the presence of ion-acoustic waves. The panels are arranged in increasing order of frequency from bottom to top. Panel (b) shows the intensity of the Langmuir waves at 36 kHz. The amplitude varies rapidly - often changing by 40 dB within one second. Panel (d) shows the amplitude levels of ion acoustic waves at 425 Hz from the low frequency SFR. Panel (c) shows the levels of interband distortion at 3.6 kHz. Weak interband distortion occurred for only nine seconds during the period shown. This form of distortion occurs when the input signal is greater than 30 mV on the 10 mV scale in the high frequency SFR. Certainly at these times we would expect to find significant harmonic distortion. Generally, that is the case, although there are some exceptions near 0715:35 UT. Panel (a) shows the intensity of the harmonic of the Langmuir waves. It shows a very erratic behavior with frequent variations of 40 dB in one second. The important point to note is that some of these increases are not accompanied by interband distortion. In particular, the enhancements of the harmonics at 0715:24 UT, and especially at 0715:50 UT, exceed 2.8 volts output without a simultaneous increase in the interband distortion. In fact, at 0715:50 UT, the maximum intensity does not appear exactly at the harmonic, but 6 kHz above the harmonic. The spectrum for this time period is shown in Figure 5. We take the spectral width of the harmonic to be the best evidence that the enhanced levels at the harmonic at this time are natural signals in the environment detected by the plasma wave receiver and not distortion in the instrument. Because of the rapid changes in the intensities of all of the waves involved in this process, it was sometimes

11

necessary to examine the spectrum on a second by second basis to separate the instrumental effects from the natural nonlinearities.

We interpret the natural enhancement at the harmonic of the Langmuir wave frequency to be transverse waves generated by the coalescence process:

$$L + L' = T$$

We would not expect there to be an exact correlation among the three waves because the transverse waves are electromagnetic and can travel long distances compared with the Langmuir waves and the ion acoustic waves which are most likely produced locally. The rapid changes in the amplitude of the Langmuir waves also obviate a detailed correlation with the other waves.

In the data analyzed to date, there are several instances where the Langmuir waves suddenly increase in intensity and remain at relatively high levels for several seconds at a time, but they do not exceed the 0 dB limit that produces instrumental nonlinearities. All three waves, Langmuir, acoustic, and transverse, increase in intensity essentially simultaneously on the one second time scale of the measurement.

Such relatively weak examples can be used to roughly estimate an intensity matrix for the process. Table 1 shows one example of intensities measured on October 31, 1984 at 0840 UT.

Table 1. The Intensity of the Langmuir (L), Acoustic (S), and Transverse (T) Waves at 0840 UT on October 31, 1984. Each Amplitude is Taken from the Channel with the Maximum Amplitude for the Corresponding Wave Mode.

$$L = 6.8 \times 10^{-4} \text{ mV/m/sqrt(Hz)}$$

$$S = 1.8 \times 10^{-4} \text{ mV/m/sqrt(Hz)}$$

$$T = 0.4 \times 10^{-4} \text{ mV/m/sqrt(Hz)}$$

These should not be taken as a rigorous measure of the strength of the process. The emission levels in the interaction region will almost certainly saturate the receiver in the high sensitivity range used during the time period of these observations. The lower levels above are most likely due to waves that have propagated some distance from the interaction region.

Another example is shown in Figure 6. Here there appear to be two types of acoustic waves. The waves generated by the decay process "rise" from the bottom of the spectrogram in the bottom panel. They are strongest after 1413 UT in the figure. Other waves, which also appear to be acoustic waves at the left and right end of the middle panel, seem to "fall" from the Langmuir waves in the top panel. All of the observations that we attribute to the decay process have been associated with the lower frequency waves that generally decrease in intensity with increasing frequency. The two types of acoustic waves are generally not observed simultaneously. Onsager et al.[7] have identified the waves that extend down from the plasma frequency as beam-driven electron acoustic waves. These waves occur coincident with increases in energetic (>9 keV) proton fluxes. The plasma data from the AMPTE quick-look survey plots show a clear correlation between the electron acoustic waves and the presence of energetic ions. In that data we find an anti-correlation between the presence of the ion acoustic waves associated with the enhanced Langmuir waves and the energetic ions.

Filbert and Kellogg[8] showed that the amplitude of electrostatic noise near the plasma frequency was strongest for field lines that are nearly tangent to the earth's bow shock, and that the amplitude diminished as the depth of penetration increased. The depth of penetration was measured by a parameter which they called DIFF, which has the units of earth radii. A model paraboloid was used to represent the shape of the bow shock. When the magnetic field line passing through the satellite intersects the bow shock, DIFF is defined as positive, and it is the distance along the X axis in GSE coordinates that the field line must be translated until it is tangent to the model shock paraboloid. If the field line does not intersect the model paraboloid, DIFF is negative. We have computed DIFF using the same model paraboloid for 21 cases when the nonlinear decay process was observed. Low resolution summary plots were used to obtain the azimuth and elevation of the magnetic field in GSE coordinates. The accuracy of DIFF is estimated to be ~ 3 Re. Figure 7 shows a histogram for the value of DIFF for these 21 cases. Almost all of the values lie between 4 and 10 Re. Only one negative value occurs, -2.85 Re. That is relatively small and probably indicates that the satellite is close to

13

the tangent line. The two very large values occurred for unusually large magnetic field azimuths near 2000.

Comparing these values of DIFF with the the electric field observations as a function of DIFF (Figure 4 of Kellogg and Filbert),[8] we find that they are in the region where the bulk of the plasma frequency emissions were observed by Kellogg and Filbert. The field amplitudes for values of DIFF between -2 and +2 Re were one to two orders of magnitude larger than for DIFF in the range from 4 to 10 Re.

We must emphasize that these results are based on a model paraboloid. Since the actual shock position varies by several earth radii, we believe that the results only indicate that the process occurs within the electron fore-shock region in front of the bow shock.

IV. DISCUSSION

The ion acoustic waves described in this report differ in the solar wind from those reported previously[5] in that they are not associated with either ion beams or a dispersed ion distribution. They occur in conjunction with enhancements of waves at the electron plasma frequency and are strongest in the electron foreshock region.

Filbert and Kellogg[8] show that the enhancements of the waves at the electron plasma frequency can be caused by a double-peaked, electron-velocity distribution arising from the reflection of solar wind electrons from the bow shock. Since this double-peaked distribution does not resonate directly with the ion-acoustic waves, it is not a direct source of energy for the ion acoustic waves. Although it is conceivable that there is another mechanism generating the ion acoustic waves at the same time the Langmuir waves are enhanced, we prefer the simpler explanation that the ion acoustic waves are being generated by the down-conversion process. A more detailed measurement of the frequency-wave number spectrum is required to definitively verify this hypothesis.

REFERENCES

1. Hoang, S., J. Fainberg, J. L. Steinberg, R. G. Stone, and R. H. Zwickl, "The 2fp Circumterrestrial Radio Emission as Seen from ISEE 3," _J. Geophys. Res._, 86, 4531 (1981).

2. Melrose, D. B., "The Emission Mechanisms for Solar Radio Bursts," _Space Sci. Rev._, 26, 3 (1980).

3. Ginzburg, V. L., and V. V. Zheleznyakov, "On the Possible Mechanisms of Sporadic Radio Emissions (Radiation in an Isotropic Plasma)," _Sov. Astron._, 653 (1958).

4. Cairns, I. H., and D. B. Melrose, "A Theory for 2fp Radiation Upstream of the Earth's Bow Shock," _J. Geophys. Res._, 90, 6637 (1985).

5. Anderson, R. R., G. K. Parks, T. E. Eastman, D. A. Gurnett, and L. A. Frank, "Plasma Waves Associated with Energetic Particles Streaming into the Solar Wind from the Earth's Bow Shock," _J. Geophys. Res._, 86, 4493 (1981).

6. Häusler, B., R. R. Anderson, D. A. Gurnett, H. C. Koons, R. H. Holzworth, O. H. Bauer, R. Treumann, K. Gnaiger, D. Odem, W. B. Harbridge, and F. Eberl, "The Plasma Wave Instrument on Board the AMPTE IRM Satellite," _IEEE Trans. Geosci. and Remote Sensing_, GE-23, 267 (1985).

7. Onsager, T., R. Holzworth, D. A. Gurnett, R. R. Anderson, O. H. Bauer, G. Haerendel, H. C. Koons, and C. Carlson, "Beam-driven Electron Acoustic Waves in the Solar Wind," _Trans. Am. Geophys. Un. (EOS)_, 66, 1032 (1985).

8. Filbert P. C. and P. J. Kellogg, "Electrostatic Noise at the Plasma Frequency Beyond the Earth's Bow Shock," _J. Geophys. Res._, 84, 1369 (1979).

17

Figure Captions

Figure 1.   Plasma Wave Spectrogram from the Swept Frequency Receiver on
             November 15, 1984. All three panels contain data from the
             electric field antenna.

Figure 2.   Plasma Wave Spectrogram from the Swept Frequency Receiver on
             September 20, 1984. The top two panels contain data from the
             electric field antenna and the bottom panel contains data from the
             magnetic field antenna. Note that the bottom two panels cover the
             same frequency range.

Figure 3.   Plasma Wave Spectrogram from the Wide-band Analog Receiver on
             September 20, 1984.

Figure 4.   Data from Four Channels of the Swept Frequency Receiver for a 100-
             s Period on October 31, 1984. The Langmuir waves occur at 36 kHz
             (b), the ion acoustic waves occur at 425 Hz (d), the transverse
             waves occur at 72 kHz (a), and interband distortion appears at 3.6
             kHz (c). The sample rate is one sample per second for (a), (b)
             and (c), and one sample every two seconds for (d).

Figure 5.   Receiver Output as a Function of Channel Number for a Single Scan
             at 0715:50 UT on October 31, 1984. The upper curve is from the
             high-frequency band from 9 to 99 kHz. The signal to the left,
             maximizing in channel 10, is from the Langmuir waves and the peak
             to the right, maximizing in channel 21, is from the transverse
             waves. The lower curve is from the low-frequency band from 0.2 to
             2.5 kHz. The ion-acoustic spectrum for this time period reaches
             up to 950 Hz, channel 13.

Figure 6.   Plasma Wave Spectrogram from the Swept Frequency Receiver on
             October 4, 1984. All three panels contain data from the electric
             field antenna.

Figure 7.   Histogram of the Number of Occurrences of Nonlinear Decay
             Processes as a Function of DIFF for 21 Time Periods When the Waves
             Were Observed by the Plasma Wave Receiver on the AMPTE IRM.
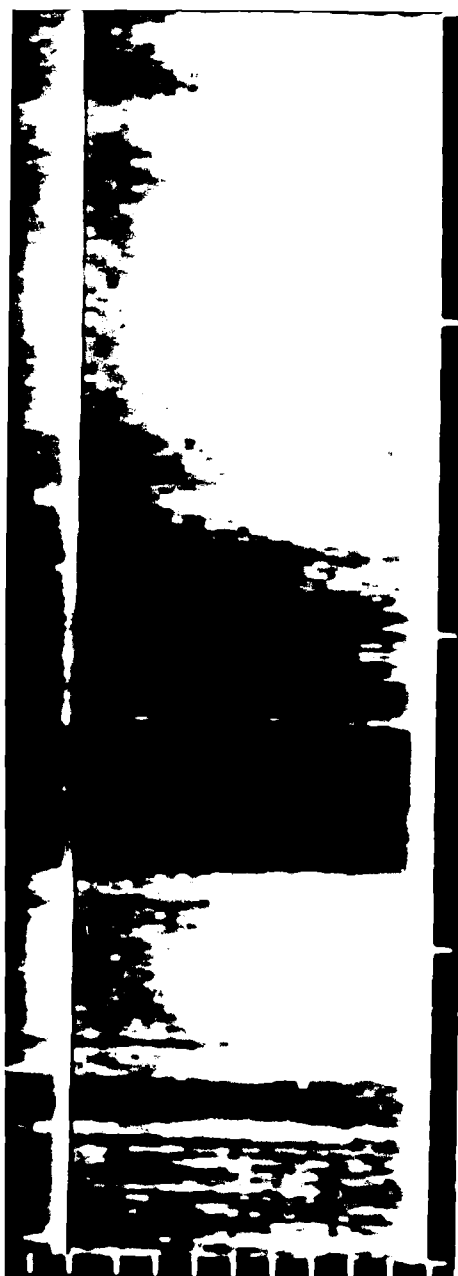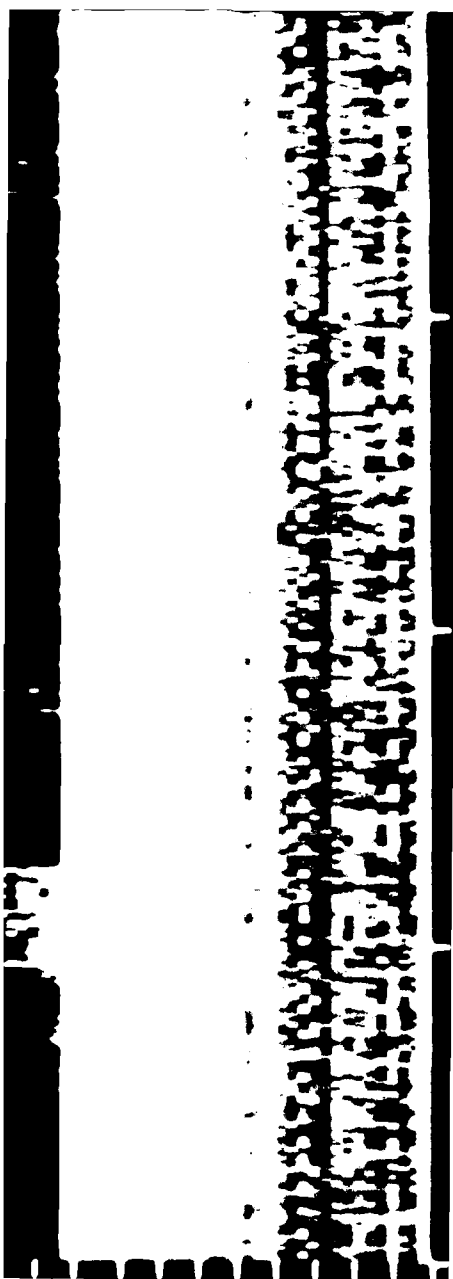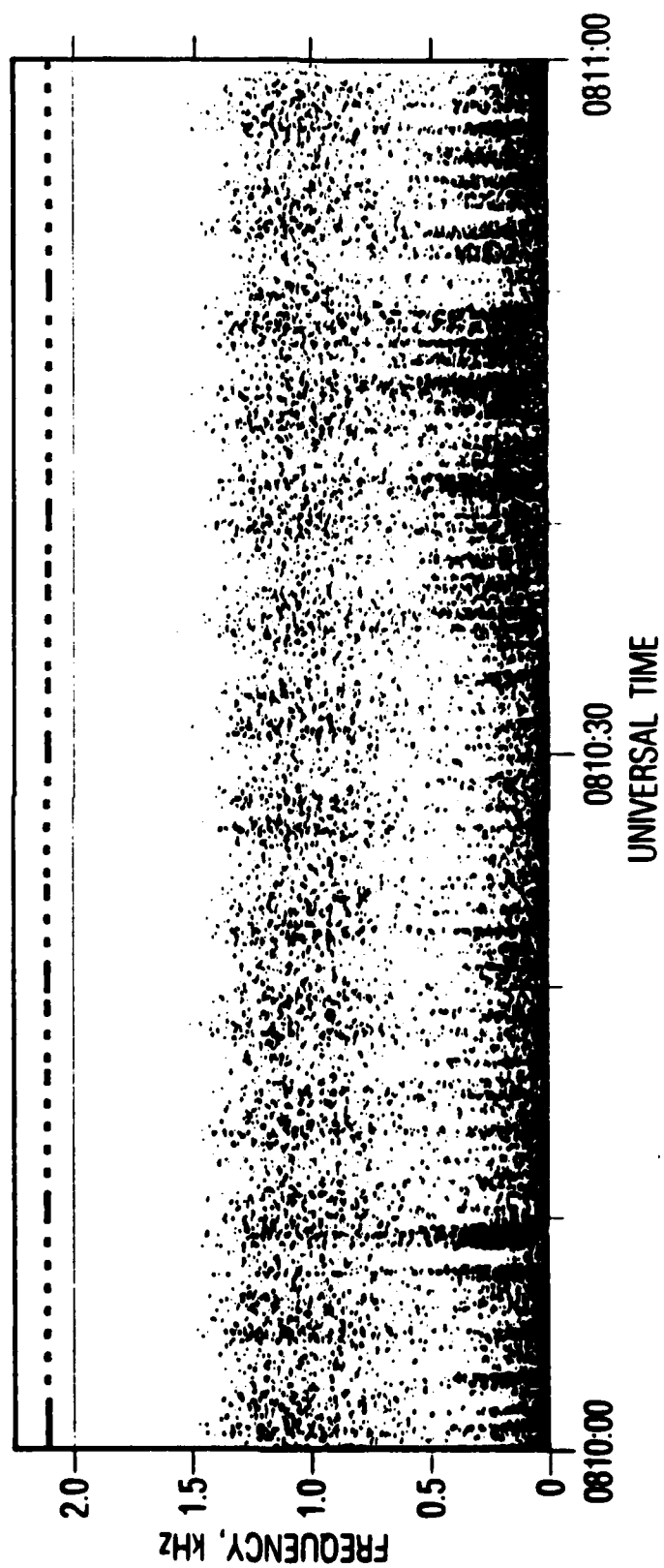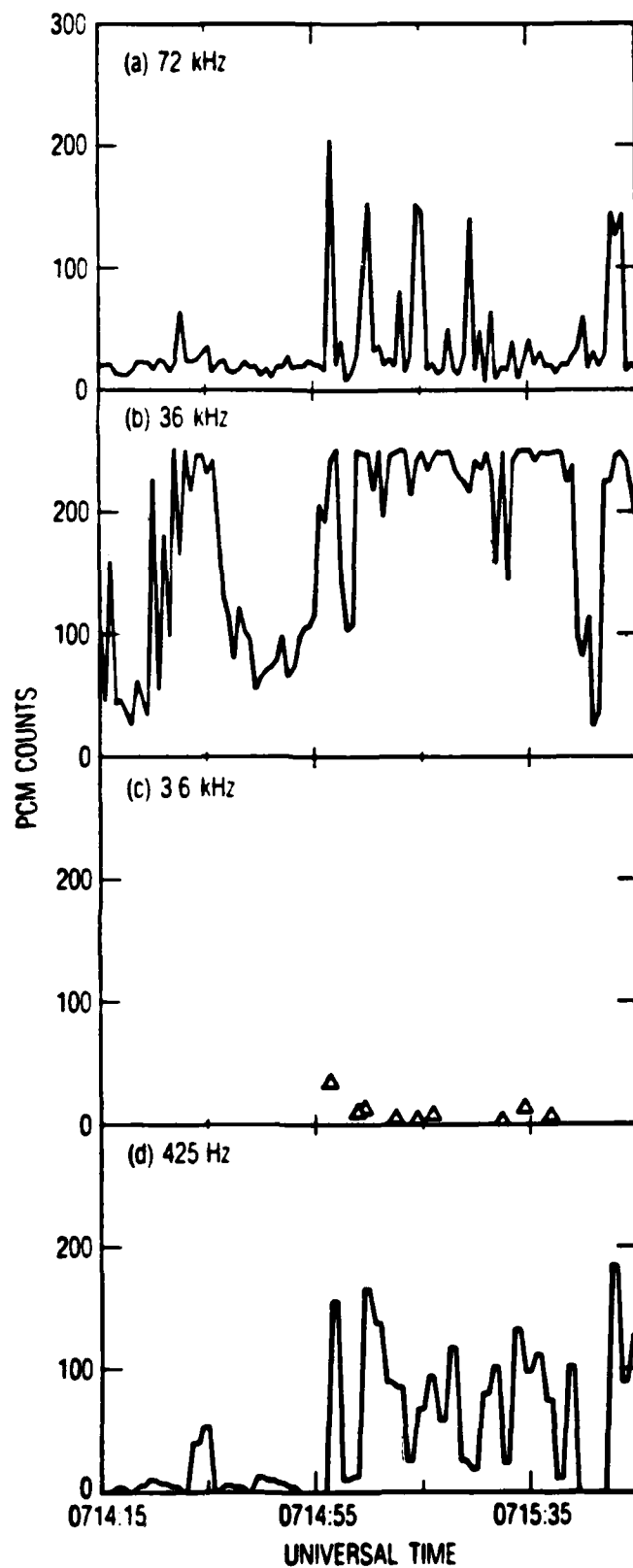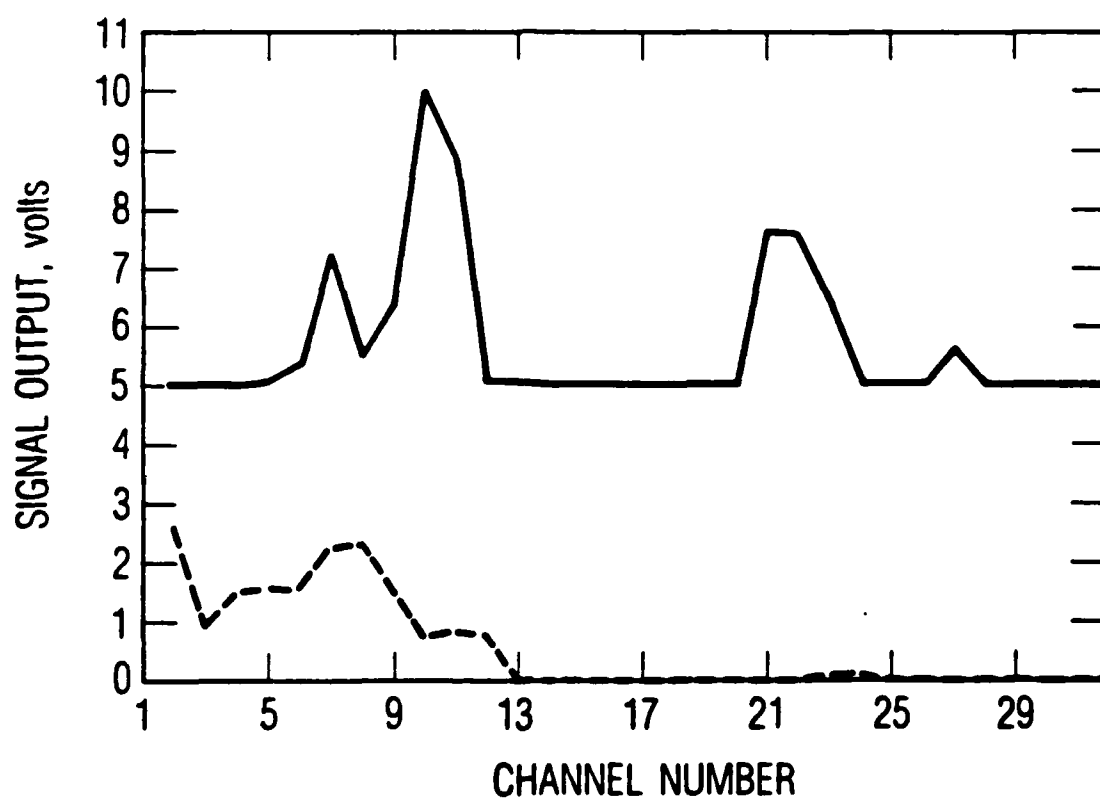
Figure 3

Figure 4

Figure 5

29

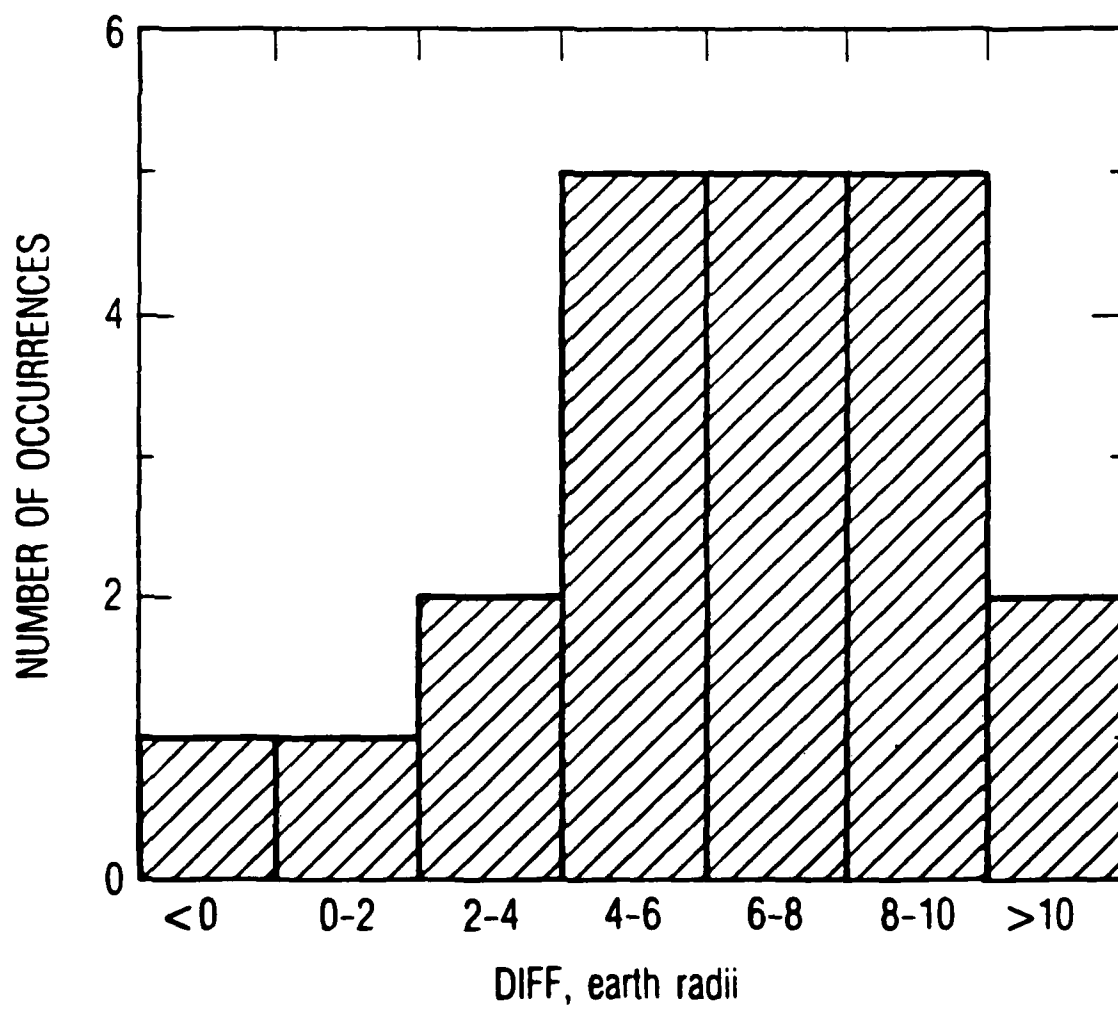AMPTE SWEPT FREQUENCY RECEIVER   4 OCT 1984

VOLT/M/SQRT(HZ)

Figure 7

33

LABORATORY OPERATIONS

The Aerospace Corporation functions as an "architect-engineer" for
national security projects, specializing in advanced military space systems.
Providing research support, the corporation's Laboratory Operations conducts
experimental and theoretical investigations that focus on the application of
scientific and technical advances to such systems. Vital to the success of
these investigations is the technical staff's wide-ranging expertise and its
ability to stay current with new developments. This expertise is enhanced by
a research program aimed at dealing with the many problems associated with
rapidly evolving space systems. Contributing their capabilities to the
research effort are these individual laboratories:

Aerophysics Laboratory: Launch vehicle and reentry fluid mechanics, heat
transfer and flight dynamics; chemical and electric propulsion, propellant
chemistry, chemical dynamics, environmental chemistry, trace detection;
spacecraft structural mechanics, contamination, thermal and structural
control; high temperature thermomechanics, gas kinetics and radiation; cw and
pulsed chemical and excimer laser development including chemical kinetics,
spectroscopy, optical resonators, beam control, atmospheric propagation, laser
effects and countermeasures.

Chemistry and Physics Laboratory: Atmospheric chemical reactions,
atmospheric optics, light scattering, state-specific chemical reactions and
radiative signatures of missile plumes, sensor out-of-field-of-view rejection,
applied laser spectroscopy, laser chemistry, laser optoelectronics, solar cell
physics, battery electrochemistry, space vacuum and radiation effects on
materials, lubrication and surface phenomena, thermionic emission, photo-
sensitive materials and detectors, atomic frequency standards, and
environmental chemistry.

Computer Science Laboratory: Program verification, program translation,
performance-sensitive system design, distributed architectures for spaceborne
computers, fault-tolerant computer systems, artificial intelligence, micro-
electronics applications, communication protocols, and computer security.

Electronics Research Laboratory: Microelectronics, solid-state device
physics, compound semiconductors, radiation hardening; electro-optics, quantum
electronics, solid-state lasers, optical propagation and communications;
microwave semiconductor devices, microwave/millimeter wave measurements,
diagnostics and radiometry, microwave/millimeter wave thermionic devices;
atomic time and frequency standards; antennas, rf systems, electromagnetic
propagation phenomena, space communication systems.

Materials Sciences Laboratory: Development of new materials: metals,
alloys, ceramics, polymers and their composites, and new forms of carbon; non-
destructive evaluation, component failure analysis and reliability; fracture
mechanics and stress corrosion; analysis and evaluation of materials at
cryogenic and elevated temperatures as well as in space and enemy-induced
environments.

Space Sciences Laboratory: Magnetospheric, auroral and cosmic ray
physics, wave-particle interactions, magnetospheric plasma waves; atmospheric
and ionospheric physics, density and composition of the upper atmosphere,
remote sensing using atmospheric radiation; solar physics, infrared astronomy,
infrared signature analysis; effects of solar activity, magnetic storms and
nuclear explosions on the earth's atmosphere, ionosphere and magnetosphere;
effects of electromagnetic and particulate radiations on space systems; space
instrumentation.

...

END

DATE
FILMED
5-88
DTIC